Cell
PRESS

Open
ACCESS

DnaK Functions as a Central Hub in the *E. coli* Chaperone Network

Giulia Calloni,[1,4] Taotao Chen,[1,4] Sonya M. Schermann,[1,5] Hung-chun Chang,[1,6] Pierre Genevaux,[2] Federico Agostini,[3] Gian Gaetano Tartaglia,[3] Manajit Hayer-Hartl,[1,*] and F. Ulrich Hartl[1,*]
[1]Department of Cellular Biochemistry, Max Planck Institute of Biochemistry, 82152 Martinsried, Germany
[2]Laboratoire de Microbiologie et Génétique Moléculaire, Centre National de la Recherche Scientifique and Université Paul Sabatier, F-31000 Toulouse, France
[3]Centre for Genomic Regulation and Universitat Pompeu Fabra, 08003 Barcelona, Spain
[4]These authors contributed equally to this work
[5]Present address: Micromet, Staffelseestr 2, 81477 Munich, Germany
[6]Present address: Department of Biology, Massachusetts Institute of Technology, Cambridge, MA 02139, USA
*Correspondence: mhartl@biochem.mpg.de (M.H.-H.), uhartl@biochem.mpg.de (F.U.H.)
DOI 10.1016/j.celrep.2011.12.007

SUMMARY

Cellular chaperone networks prevent potentially toxic protein aggregation and ensure proteome integrity. Here, we used *Escherichia coli* as a model to understand the organization of these networks, focusing on the cooperation of the DnaK system with the upstream chaperone Trigger factor (TF) and the downstream GroEL. Quantitative proteomics revealed that DnaK interacts with at least ~700 mostly cytosolic proteins, including ~180 relatively aggregation-prone proteins that utilize DnaK extensively during and after initial folding. Upon deletion of TF, DnaK interacts increasingly with ribosomal and other small, basic proteins, while its association with large multidomain proteins is reduced. DnaK also functions prominently in stabilizing proteins for subsequent folding by GroEL. These proteins accumulate on DnaK upon GroEL depletion and are then degraded, thus defining DnaK as a central organizer of the chaperone network. Combined loss of DnaK and TF causes proteostasis collapse with disruption of GroEL function, defective ribosomal biogenesis, and extensive aggregation of large proteins.

INTRODUCTION

In all cell types, molecular chaperones function in preventing protein misfolding and aggregation, typically by shielding hydrophobic surfaces exposed by proteins in their non-native states. Chaperones have essential roles in assisting the folding, assembly and transport of newly synthesized polypeptides and in surveying the conformational status of preexistent proteins (Hartl and Hayer-Hartl, 2009). Although detailed insights into the structure and mechanism of individual chaperone components have been obtained in recent years, how multiple chaperone modules cooperate to maintain conformational proteome integrity (proteostasis) is not yet understood (Balch et al., 2008).

What is the degree of functional overlap and specificity among chaperones, and how robust is the network in tolerating disturbances and avoiding collapse? Although there is evidence that the complexity of proteostasis networks has increased during evolution (Gidalevitz et al., 2011), central players, such as the ATP-regulated Hsp70 chaperones, have been highly conserved from bacteria to human. Here we employed quantitative proteomics to analyze the chaperone network of *Escherichia coli* as a tractable model, focusing on the central role of the Hsp70 system.

DnaK, the major bacterial Hsp70, is one of the most abundant constitutively expressed and stress inducible chaperones in the *E. coli* cytosol. Yet it is not essential under nonstress conditions at intermediate temperature (Bukau and Walker, 1989). Indeed, DnaK (together with its co-chaperone DnaJ and regulator GrpE) cooperates in de novo protein folding with the ribosome-bound chaperone Trigger factor (TF). Although DnaK and TF can be deleted individually, their simultaneous deletion results in synthetic lethality at temperatures above 30°C (Deuerling et al., 1999; Genevaux et al., 2004; Teter et al., 1999). Under stress conditions, such as heat shock at 42°C, DnaK becomes indispensable (Bukau and Walker, 1989). TF and DnaK act upstream of the essential GroEL/ES chaperonin, which provides a cage-like compartment for the folding of single protein molecules, unimpaired by aggregation. About 10% of cytosolic proteins (~250 different proteins) have been found to interact with GroEL, of which a subset of ~50−85 proteins (so-called class III substrates) are absolutely GroEL/ES dependent for folding (Fujiwara et al., 2010; Kerner et al., 2005).

The ATP-dependent reaction cycle of DnaK is regulated by the Hsp40 co-chaperone DnaJ and the nucleotide exchange factor GrpE (reviewed in Hartl et al., 2011; Mayer, 2010). DnaJ functions in presenting non-native substrate proteins to DnaK (Figure 1A). Substrate binding and release by Hsp70 is achieved through the allosteric coupling of a N-terminal ATPase domain with a C-terminal peptide-binding domain, the latter consisting of a β sandwich subdomain and an α-helical lid segment. The β sandwich recognizes extended, ~7 residue segments enriched with hydrophobic amino acids, preferentially when they are framed by positively charged residues (Rüdiger et al., 1997; Zhu et al.,
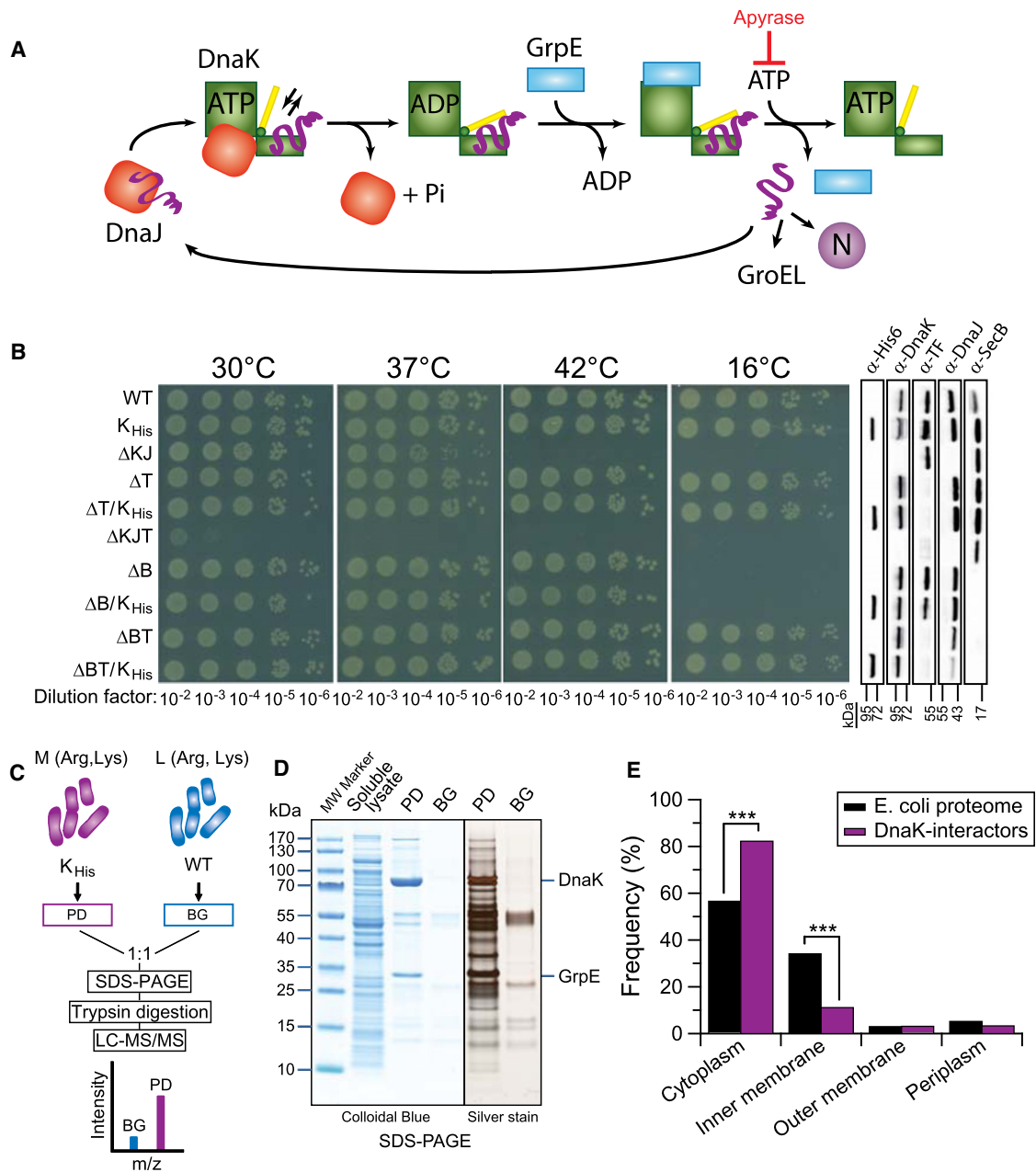
Figure 1. Isolation of DnaK-Interactor Complexes

(A) Schematic representation of the DnaK reaction cycle. Upon DnaJ-mediated delivery of non-native protein substrate to ATP-bound DnaK, hydrolysis of ATP to ADP results in closing of the α-helical lid (yellow) and tight binding of substrate by DnaK. Stable DnaK-substrate complexes are accumulated by depleting ATP with apyrase upon cell lysis.

(B) In vivo functionality of the chromosomally encoded DnaK-His6. The *dnaK* gene (WT) was replaced with *dnaK-His6* (K$_{His}$) in MC4100 and where indicated in the isogenic chaperone mutant strains Δ*dnaKdnaJ* (ΔKJ), Δ*tig* (ΔT), Δ*tig/dnaK-His6* (ΔT/K$_{His}$), Δ*dnaKdnaJtig* (ΔKJT), Δ*secB* (ΔB), Δ*secB/dnaK-His6* (ΔB/K$_{His}$), Δ*secBΔtig* (ΔBT), and Δ*secBΔtig/dnaK-His6* (ΔBT/K$_{His}$) as described in Extended Experimental Procedures. Cells in mid-log phase were serially diluted, spotted on LB agar plates and incubated for 1 day at 30°C, 37°C, or 42°C and for 5 days at 16°C.

(C) Schematic of the SILAC approach used to identify DnaK interactors. L (light) and M (medium) Arg, Lys isotope media. DnaK-substrate complexes isolated from M-labeled cells containing the DnaK-His6 (pulldown, PD) were mixed 1:1 with L-labeled proteins isolated with the same procedure from an equal amount of cell lysate containing non-tagged DnaK (background, BG). The mixture was subsequently separated by SDS-PAGE, followed by in-gel trypsin digestion and LC-MS/MS analysis.

(D) Isolation of DnaK-substrate complexes. Soluble lysate, PD and BG fractions were analyzed by 4%−12% gradient SDS-PAGE, followed by Colloidal Blue or silver staining, as indicated.

(E) Cellular localization of DnaK interactors compared to the genome-based *E. coli* proteome (Yu et al., 2011). ***p ≤ 0.001 based on χ^2 test.

1996). The α-helical lid and a conformational change in the β sandwich domain regulate the affinity state for peptide through an ATP-dependent, allosteric mechanism (Zhuravleva and Gierasch, 2011). In the ATP-bound state, the lid adopts an open conformation, resulting in high on- and off-rates for peptide (Figure 1A). Hydrolysis of ATP to ADP is accelerated by DnaJ, leading to lid closure and stable peptide binding. Following ATP-hydrolysis, DnaJ dissociates and GrpE binds to the DnaK ATPase domain, catalyzing ADP release. Binding of ATP then results in lid-opening and substrate release for folding or transfer to other chaperones (Figure 1A).

Attempts to identify DnaK substrates have been limited to the analysis of proteins that aggregated in cells lacking TF upon depletion of DnaK (Deuerling et al., 2003). Here we developed an approach for the direct isolation of DnaK-substrate complexes and their identification by quantitative proteomics from wild-type, TF-deleted, or GroEL-depleted cells. In parallel, we analyzed global proteome changes under conditions of single or combined chaperone deletion. Our measurements show that DnaK normally interacts with at least ~700 newly synthesized and preexistent proteins, which we characterized based on their relative enrichment on DnaK. Individual deletion of TF or depletion of GroEL/ES leads to specific changes in the DnaK interactome and in global proteome composition. These effects are highly informative as to the functional cooperativity of chaperone modules. We conclude that DnaK is the central hub in the cytosolic *E. coli* chaperone network, interfacing extensively with the upstream TF and the downstream chaperonin. The functional interconnection of these major chaperone systems is critical for robust proteostasis control.

RESULTS

Isolation and Identification of the DnaK Interactome
To isolate DnaK-substrate complexes, we generated an *E. coli* MC4100 strain in which the wild-type *dnaK* gene was replaced by *dnaK-His6*, encoding DnaK with a C-terminal His6-tag (henceforth called K_{His}). K_{His} cells grew like wild-type (WT) on agar plates or in liquid culture at 30°C–37°C, or under heat shock conditions at 42°C (Figure 1B and Figure S1A available online). Quantitative proteomic analysis using SILAC (stable isotope labeling with amino acids in cell culture) (Ong et al., 2002) did not detect significant differences in protein abundance between WT and K_{His} cells (Figure S1B). DnaK-His6 also supported normal growth of TF-deleted (ΔT) cells above 30°C and of cells lacking the protein export chaperone SecB (ΔB) (Figure 1B and Figure S1A) (Deuerling et al., 1999; Genevaux et al., 2004; Smock et al., 2010; Teter et al., 1999). ΔB cells are cold-sensitive and this defect is compensated by deletion of TF (Ullers et al., 2007).

We isolated DnaK interactors by immobilized metal affinity chromatography (IMAC) from K_{His} cells growing exponentially at 37°C. DnaK-substrate complexes were stabilized during cell lysis by rapidly (within <10 s) depleting ATP with apyrase to inhibit substrate cycling (Figure 1A) (Teter et al., 1999). The K_{His} cells were SILAC-labeled with medium (M) Arg/Lys isotopes, lysate prepared and subjected to IMAC pulldown (PD). DnaK-His6 complexes were mixed 1:1 with a background (BG) sample

obtained by the same IMAC procedure from lysate of unlabeled WT cells (light isotopes, L) (Figure 1C and Extended Experimental Procedures). The composition of PD and BG samples prior to mixing is shown in Figure 1D. Note that GrpE was co-isolated with DnaK as a stoichiometric complex (Figures 1A and 1D), whereas DnaJ was present in substoichiometric amounts (Table S1). The molar ratio of DnaK/GrpE/DnaJ was ~30:20:1, as estimated from the number of peptides identified by MS using exponentially modified Protein Abundance Index (emPAI) scores (Ishihama et al., 2005).

A total of 674 DnaK interactors (Table S1) were identified by LC-MS/MS with >95% confidence (Figure S1C and Extended Experimental Procedures), including proteins either not identified in BG samples or having a >2-fold enrichment (M/L ratio) in PD over BG in at least two of three independent experiments (biological repeats). Most of these (503 proteins) were >4-fold enriched over BG (Table S1). The identification of DnaK interactors approached saturation in consecutive experiments (Extended Experimental Procedures). For the vast majority of interactors (>95%), the amount of protein co-isolated with DnaK was strongly diminished upon incubation of cell lysate with ATP (Figure S1D), indicating that these proteins bind DnaK in an ATP-regulated manner. While GrpE was released, DnaJ was enriched on DnaK in the presence of ATP (data not shown) (Figure 1A). The DnaJ homolog cbpA and the two small heat shock proteins, IbpA and IbpB (Hsp20), were also identified in DnaK pulldowns in the presence of ATP, suggesting that these chaperones functionally cooperate with DnaK (data not shown).

Approximately 80% of the DnaK interactors are predicted to be cytosolic, ~11% are inner membrane proteins, ~3% outer membrane proteins, and ~3% are located in the periplasm (Figure 1E and Table S1). Thus, the identified DnaK interactors comprise ~25% of the cytosolic proteome. As a collective, they are similar to a set of 1,938 proteins identified in soluble cell lysates (list available at the Proteome Commons Tranche repository) in terms of molecular weight (Figure S1E) and other physico-chemical properties, such as isoelectric point, average hydrophobicity, and aggregation propensity (data not shown), indicating that DnaK has a broad substrate specificity.

Classification of DnaK Substrates by Enrichment on DnaK
We next analyzed each of the different DnaK interactors to determine what fraction of the total protein is DnaK-bound, assuming that this parameter correlates with chaperone dependence, as was observed for the substrates of GroEL (Kerner et al., 2005). Unlabeled soluble cell lysate (L) was mixed at a defined proportion with DnaK complexes isolated from cells labeled with heavy Arg/Lys isotopes (H) and H/L ratios were determined by LC-MS/MS. H/L ratios were obtained for 666 DnaK interactors, reflecting their relative enrichment on DnaK. The relative enrichment factors (REF) displayed a broad, bimodal distribution (Figure 2A). By setting thresholds at the 20th and 70th percentiles of the distribution, we grouped 142 proteins as less-enriched, 183 proteins as enriched, and 341 proteins as medium enriched on DnaK (Figure 2A and Table S1). Interestingly, the enriched proteins are below average in cellular abundance but together make up ~40% of all identified DnaK interactors by mass
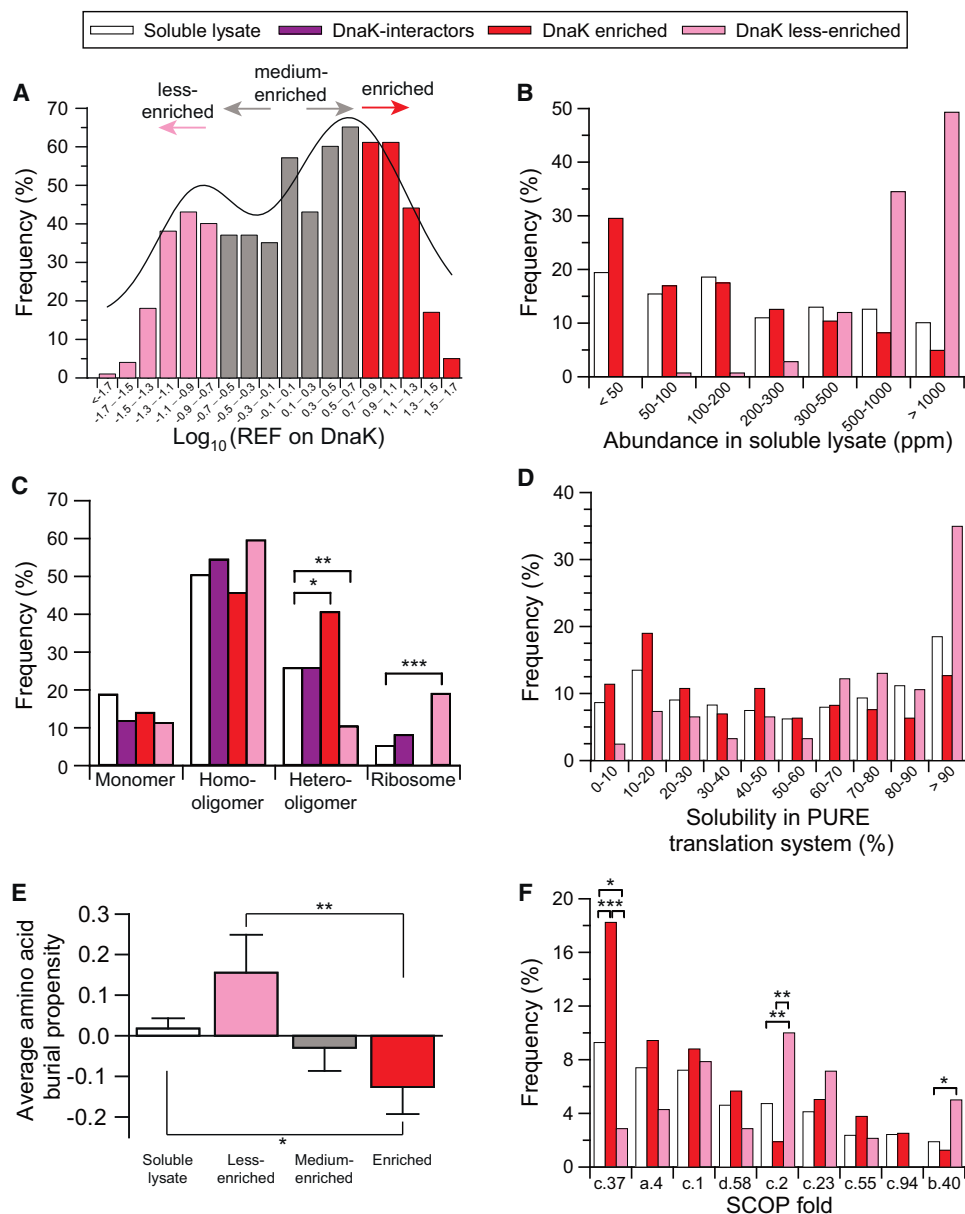
Figure 2. Classification and Characterization of DnaK Interactors

(A) Relative enrichment of interactor proteins on DnaK. The histogram shows the distribution of relative enrichment factors (REF) for 666 DnaK interactors identified in 3 independent experiments. REF indicates the fraction of total cellular protein bound to DnaK. Enriched and less-enriched sets of interactors were selected at the extremes of the distribution for further analysis as described in Extended Experimental Procedures.

(B–F) Properties of enriched and less-enriched DnaK interactors compared to soluble lysate proteins. (B) Abundance in soluble lysate determined based on cumulative abundance values (emPAI) (Ishihama et al., 2005). (C) Oligomeric state of all, the enriched and less-enriched DnaK interactors compared to lysate proteins. Ribosomal proteins are analyzed separately. (D) Solubility upon in vitro translation in the absence of chaperones (Niwa et al., 2009). (E) Average propensity of soluble lysate proteins and DnaK interactors to bury amino acid residues from solvent, calculated using the burial propensity scale of specific amino acids by Janin (1979) (see Extended Experimental Procedures). Shown is the mean burial propensity for each class; error bars correspond to the SEM. P values based on Mann-Whitney test: *$p \leq 0.05$; **$p \leq 0.01$. (F) SCOP fold distribution. c.37, P loop containing nucleotide triphosphate hydrolases; a.4, DNA/RNA binding 3-helical bundle; c.1, TIM β/α barrel; d.58, Ferredoxin-like; c.2, NAD(P)-binding Rossmann-fold domains; c.23, Flavodoxin-like; c.55, Ribonuclease H-like motif; c.94, Periplasmic binding protein-like II; b.40, OB-fold. Statistical significance for categorical variables is based on a χ^2 test: *$p \leq 0.05$; **$p \leq 0.01$; ***$p \leq 0.001$.

(Figure 2B and Table S1), as based on emPAI scores. For these proteins ~5% of cellular content is bound to DnaK. In contrast, the less-enriched DnaK interactors are highly abundant proteins but amount to only ~13% of all DnaK interactors by mass (Figure 2B and Table S1). On average, only 0.1% or less of their cellular content is DnaK-bound. The medium enriched

interactors amount to ~47% of all DnaK interactors by mass, with ~1% of cellular content being bound.

The DnaK-enriched proteins cover a wide range of cellular functions, prominently including DNA replication, recombination and repair (COG class L), and cell division and chromosome partitioning (COG class D) (Figure S2A and Table S1). The less-enriched DnaK interactors have a significant preference for proteins involved in translation, ribosomal structure, and biogenesis (COG class J) and include 24 ribosomal proteins. Essential proteins (Gerdes et al., 2003) are more frequent among the less-enriched substrates (Figure S2B). The enriched interactors include some very large proteins >100 kDa (Figure S2C) and tend to have more predicted DnaK binding sites than the less enriched substrates (both absolute and when corrected for size) (Figure S2D) (Van Durme et al., 2009). Furthermore, they are more frequently part of heterooligomeric complexes (when ribosomal proteins are considered separately) (Figure 2C).

To determine whether the proteins enriched on DnaK have a high propensity to aggregate, we took advantage of the study by Niwa et al. (2009) who analyzed the solubility of *E. coli* proteins upon in vitro translation in the absence of chaperones. Indeed, the DnaK-enriched proteins are more aggregation prone upon translation than average proteins of soluble cell lysate, whereas the less-enriched DnaK interactors are more soluble (Figure 2D). This is consistent with the finding that the enriched proteins frequently display pI values close to neutral pH (Figure S2E). Moreover, these proteins are predicted to bury amino acid residues less effectively from solvent than the less enriched DnaK interactors and average soluble proteins (Figure 2E) (Tartaglia et al., 2010). This suggests that the enriched interactors populate dynamic intermediate states during folding and expose hydrophobic residues, although their average sequence hydrophobicity is not increased (data not shown). Similar properties were previously found for the obligate (class III) GroEL substrates (Figure 2E) (Raineri et al., 2010; Tartaglia et al., 2010). Interestingly, ~18% (29 proteins) of the DnaK-enriched substrates with assigned fold (159 proteins) contain at least one domain with SCOP fold c.37 (P loop containing nucleoside triphosphate hydrolases), compared to only ~8% of soluble lysate proteins and ~3% of the less-enriched DnaK interactors (Figure 2F). The c.37 fold is characterized by a complex α/β topology and is highly represented in heterooligomeric proteins (Figure S2F). The less-enriched substrates have a preference for the SCOP folds c.2 (NAD(P)-binding Rossmann-fold) and b.40 (OB-fold) (Figure 2F), which are found in abundant metabolic enzymes and in ribosomal proteins, respectively.

In summary, the relative enrichment of proteins on DnaK correlates with their propensity to aggregate during folding. The ~180 most enriched DnaK interactors amount to ~40% of total mass of DnaK substrates. They are of relatively low cellular abundance, tend to contain more predicted DnaK binding sites than the less-enriched interactors, and frequently assemble with other proteins to heterooligomeric complexes.

Effects of DnaK Deletion at the Proteome Level

To analyze the global effects of deleting the DnaK chaperone system, we performed quantitative proteomics of Δ*dnaKdnaJ* (ΔKJ) cells (H-labeled) in comparison to K_{His} cells (M-labeled).

The cells were grown at 30°C where deletion of DnaK/DnaJ is well tolerated in liquid culture (Figure 1B and Figure S1A). Out of ~1,400 proteins quantified, 105 proteins were increased in abundance in ΔKJ cells (Table S2A). These proteins include 42 identified DnaK interactors, presumably reflecting a compensatory response. In addition, the major cytosolic chaperones and proteases (GroEL/ES, HtpG, IbpA, IbpB, ClpB, Hsp33, HslU, HslV, Lon) were upregulated 5- to >10-fold, consistent with a 4.5-fold increase in abundance of the central heat shock regulator rpoH (σ32), which is negatively controlled by DnaK and DnaJ (Table S1) (Gamer et al., 1992; Straus et al., 1990). Indeed, the genes of 56 of the 105 upregulated proteins contain known or putative σ32 binding sites in their upstream regions (Zhao et al., 2005) (Table S2A). Interestingly, 87 proteins were reproducibly reduced in abundance in ΔKJ cells by ~40%−95% (median 60%; p < 0.05) (Table S2B). SILAC pulse-labeling demonstrated similar rates of synthesis in K_{His} and ΔKJ cells (Figure S2G), indicating that the observed decrease in protein abundance was largely due to degradation. Notably, among the degraded proteins were 40 identified DnaK interactors (four essential proteins), including the periplasmic chaperones of acid-denatured proteins hdeA and hdeB, and several amino acid metabolic enzymes. The DnaK interactors that are degraded in ΔKJ cells are above average enriched on DnaK in DnaK-His6 cells (Table S2B) and exhibit relatively low solubility upon in vitro translation (Figure S2H) (Niwa et al., 2009).

To determine whether proteins aggregate in cells lacking DnaK/DnaJ, we analyzed the insoluble and soluble fractions of ΔKJ cells compared to K_{His} cells. In total, 474 proteins were significantly increased in the insoluble fraction of ΔKJ cells, including 201 identified DnaK interactors (Table S3). However, only 65 proteins were substantially depleted from the soluble fraction by 5%−90% (median ~9%; p < 0.05) due to aggregation. Among this group of proteins were 30 identified DnaK interactors (eight essential proteins), such as excision nuclease subunit A (uvrA) (Table S3). The extent of aggregation correlated strongly with enrichment on DnaK (Table S3).

These findings demonstrate that a subset of DnaK interactors are specifically dependent on the DnaK system in vivo. These proteins tend to be degraded or aggregate in ΔKJ cells, even at a growth temperature of 30°C, where the loss of DnaK is otherwise well compensated.

DnaK Interacts with Newly Synthesized and Preexistent Proteins

To determine whether proteins interact with DnaK only during initial folding or return to DnaK later for conformational maintenance (newly synthesized and preexistent interactors, respectively), we performed pulse-SILAC experiments. K_{His} cells grown at 37°C with unlabeled Arg/Lys (L) were shifted to M-labeled Arg/Lys for 2.5 min to label newly synthesized polypeptides. WT cells grown in heavy (H) Arg/Lys served as background control. Lysates from the K_{His} and WT cells were mixed 1:1 and DnaK interactors identified. The M/L ratio of a DnaK interactor relative to its M/L ratio in the lysate (the latter correcting for rates of synthesis and turnover) was used to indicate whether it bound to DnaK preferentially as a newly synthesized or preexistent protein (Figure 3A). Isotope ratios were obtained
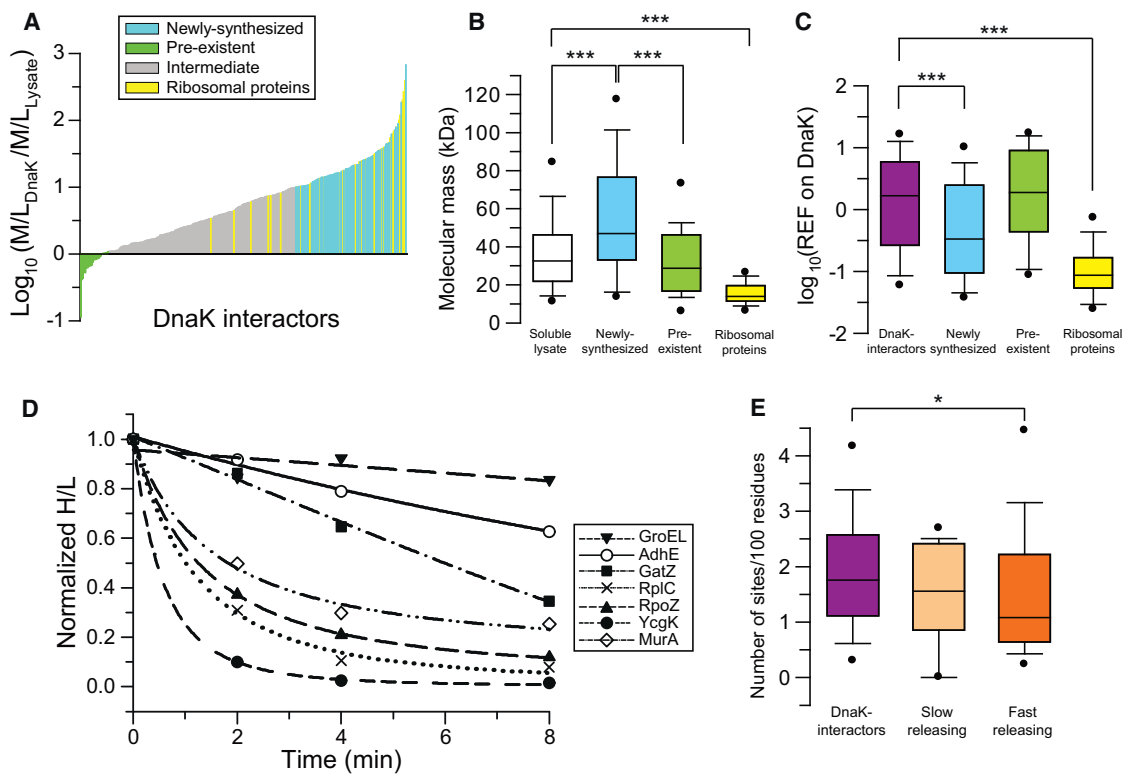
Figure 3. Characterization of Proteins that Interact with DnaK upon Synthesis or for Conformational Maintenance

(A–C) Analysis of DnaK interactors classified by pulse-SILAC as preexistent or newly synthesized proteins. (A) Ratios of medium to light isotopes (M/L) of DnaK interactors relative to the M/L ratios for the same proteins in soluble cell lysate. Positive values of the log transformed ratio of ratios indicate a preferential interaction with DnaK as newly synthesized proteins. Groups of proteins are color coded: blue and green, strong tendency to interact as newly synthesized or preexistent proteins; gray, intermediate tendency to interact as newly synthesized proteins; yellow, ribosomal proteins. Molecular weight (B) and relative enrichment factors (REF) on DnaK (C) of the substrates preferentially interacting as preexistent or newly synthesized polypeptides as compared to *E. coli* soluble lysate proteins and all DnaK interactors, respectively. The ribosomal proteins among DnaK interactors are analyzed separately. Horizontal line indicates the median, whisker caps and circles indicate 10th/90th and 5th/95th percentiles, respectively. P values based on Mann-Whitney test: ***$p \leq 0.001$.

(D and E) Time-dependent dissociation of proteins from DnaK as determined by pulse-chase SILAC. (D) Kinetics of dissociation from DnaK shown for selected proteins. Data were fitted to exponential decay. (E) Distribution of the number of predicted DnaK binding sites (Van Durme et al., 2009) for the DnaK-interactor sets with fast and slow release kinetics as compared to all DnaK interactors. Horizontal line indicates the median, whisker caps and circles indicate 10th/90th and 5th/95th percentiles, respectively. P value based on Mann-Whitney test: *$p \leq 0.05$.

for ∼300 DnaK interactors (Table S4). Log_{10} M/L ratios lower than 0, indicating a strong preference for interaction as preexistent protein, were observed for only 20 interactors (Figure 3A, green). Most other proteins bound to DnaK upon synthesis (Figure 3A, gray and blue), including ∼100 proteins with a strong preference for interaction as newly synthesized polypeptides (log_{10} M/L ratio ≥ 1) (Figure 3A, blue). Ribosomal proteins are included in this group (Figure 3A, yellow), in support of the proposed role of DnaK in ribosome assembly (Maki et al., 2002; René and Alix, 2011).

We next compared the physico-chemical properties of the newly synthesized and preexistent DnaK interactors (Figure 3A). Ribosomal proteins were analyzed separately, as their unusual size and charge properties would introduce a strong bias. Interestingly, the 71 proteins with a strong preference to interact with DnaK upon synthesis are significantly shifted to large sizes and thus are likely to have complex folding pathways (Figure 3B). They are of average to above average cellular abundance and

comparable to lysate proteins in terms of hydrophobicity and aggregation propensities, as calculated with the Z_{agg} algorithm based on their amino acid sequence properties (Tartaglia et al., 2008) (Figures S3A and S3B). Interestingly, only a few of these proteins aggregated in ΔKJ cells (Table S3), suggesting that they can utilize multiple chaperones for folding or, perhaps less likely, have only low chaperone dependence. As expected, the ribosomal proteins have very low aggregation scores, consistent with their charge character (Figure S3B). Furthermore, the tendency to interact with DnaK upon synthesis correlates with a relatively lower enrichment on DnaK, suggesting that these proteins interact only transiently (Figure 3C). On the other hand, the preexistent interactors are similar in size to the average of lysate proteins (Figure 3B) and are more enriched on DnaK than the newly synthesized substrates (Figure 3C), arguing for longer residence times on DnaK. They are also characterized by higher intrinsic aggregation propensities than the newly synthesized interactors ($p < 0.05$) (Figure S3B) and several of
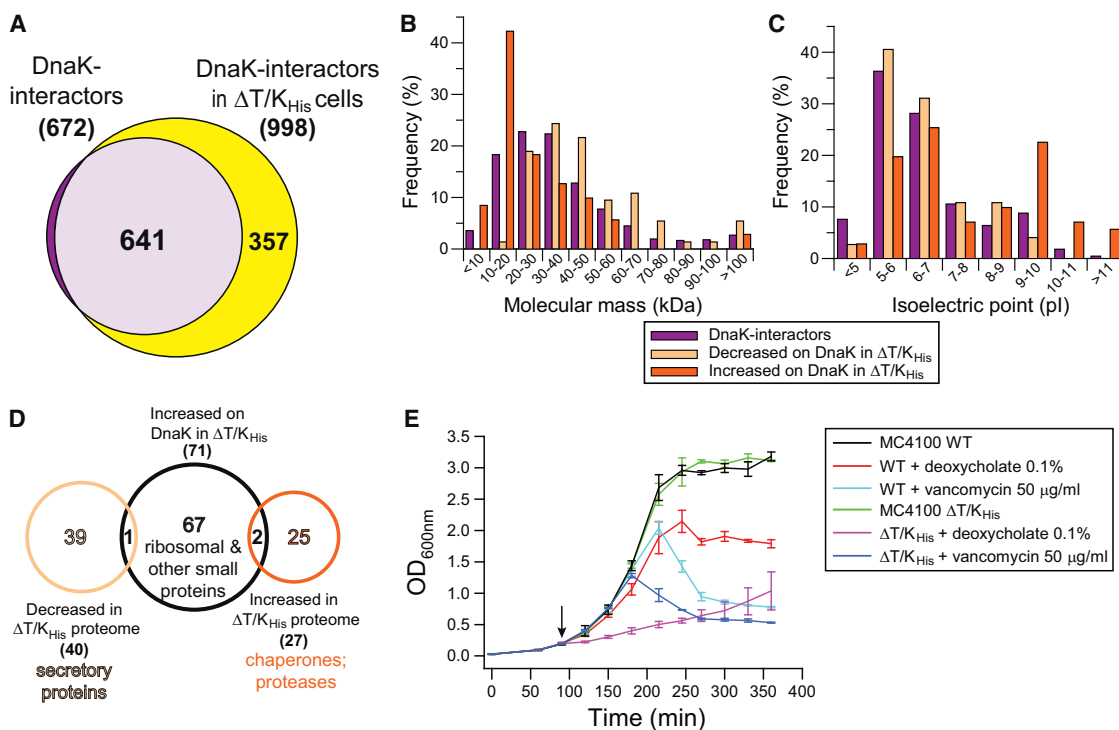
Figure 4. Effect of TF Deletion on the DnaK Interactome and Cellular Proteome

(A) Overlap of DnaK interactors in K_{His} (672 proteins) and $\Delta T/K_{His}$ cells (998 proteins).

(B and C) Change in the distribution of molecular weight (B) and isoelectric point (C) of the DnaK interactome in $\Delta T/K_{His}$ cells compared to all DnaK interactors in K_{His} cells.

(D) Minimal overlap of the sets of proteins significantly decreased or increased in abundance in the proteome of $\Delta T/K_{His}$ cells with the set of proteins that increased on DnaK in $\Delta T/K_{His}$ cells.

(E) Outer membrane destabilization in $\Delta T/K_{His}$ cells. Growth curves at 37°C of K_{His} and $\Delta T/K_{His}$ cells in the presence and absence of 0.1% deoxycholate or 50 μg/ml vancomycin. Arrow indicates the time of addition of deoxycholate or vancomycin after dilution of an overnight culture in fresh M63 medium at an OD_{600nm} of 0.025. Error bars represent SD of three independent measurements.

these proteins were found to be degraded in ΔKJ cells (Table S2B). Thus, a prominent feature of the preexistent interactors is their intrinsic tendency to populate aggregation-prone states, consistent with a requirement for conformational maintenance by DnaK.

Protein Flux through DnaK

To measure the residence time of interactors on DnaK directly, K_{His} cells were pulse-labeled with Arg/Lys isotopes (H) for 2.5 min, followed by a chase with excess unlabeled amino acids (L). Time course data based on the time-dependent decrease of the H/L ratio were collected for 91 proteins, with apparent dissociation rates from DnaK corresponding to half-times of ~30 s to ~25 min (Figure 3D and Table S5). Proteins with slow release rates (≤30th percentile of the rate distribution; 27 proteins) include GroEL, IbpA, and SecB, presumably reflecting the functional cooperation of these chaperones with DnaK. Slow releasing proteins (excluding chaperones) are characterized by above average enrichment on DnaK and an average number of predicted binding sites compared to all DnaK interactors (Figure 3E). Proteins with fast release rates (≥70th percentile of the rate distribution; 27 proteins) display

average enrichment on DnaK and tend to have a lower number of binding sites (Figure 3E). Most of these substrates are predicted to bury hydrophobic regions effectively (data not shown). Thus, the residence time (and consequently the enrichment) on DnaK appears to be regulated, at least in part, by the frequency of potential DnaK recognition motifs in the polypeptide chain and by the efficiency of their burial during folding. Fast release rates correlate generally with the tendency of proteins to interact with DnaK only upon synthesis, whereas proteins that utilize DnaK also for maintenance have longer residence times.

Partial Functional Redundancy of DnaK and TF

To understand how DnaK interfaces with other modules of the chaperone network, we first investigated how the DnaK interactome changes upon deletion of the upstream chaperone TF. We identified the DnaK interactors in the TF deletion strain at 37°C by pulldown from H-labeled Δ*tig/dnaK-His6* (ΔT/K_{His}) cells using L-labeled ΔT cells as the background. The number of identified DnaK interactors increased to 998 (see Proteome Commons Tranche repository), including ~95% of the 672 DnaK interactors identified in K_{His} cells (Figure 4A). (DnaK levels increased ~1.4-fold in ΔT/K_{His} cells; see Table S6D below.) The additional

proteins have physico-chemical properties similar to the DnaK interactors in WT cells (data not shown). To detect quantitative changes in the DnaK interactome upon TF deletion, we performed a comparative analysis of H-labeled $\Delta T/K_{His}$ and M-labeled K_{His} cells. Seventy-one proteins interacted to a significantly greater extent (1.4- to 3.3-fold) and 74 proteins to a lesser extent with DnaK in $\Delta T/K_{His}$ cells (Tables S6A and S6B). The proteins accumulating on DnaK are typically small in size (<20 kDa) (Figure 4B) and include 17 highly basic ribosomal proteins as well as ten basic nonribosomal proteins (pI $\geq$ 9) (Figure 4C), such as several secretory proteins with functions in cell envelope and outer membrane biogenesis (Skp, AmpH, YcgK, SlyB) (Table S6A). The proteins that interacted less extensively with DnaK in $\Delta T/K_{His}$ cells are larger in size (Figure 4B) and overlap with the large newly synthesized DnaK interactors described above (Figure 3B). Apparently, they bind to DnaK less efficiently in the absence of TF (Figure 4B).

We also performed a proteomic analysis of total cell lysate of $\Delta T/K_{His}$ cells as compared to K_{His} cells. Only 40 of 1,490 quantified proteins were reproducibly reduced in abundance by 25%−85% (p < 0.05) when TF was deleted (Table S6C), although their rates of synthesis were unchanged (Figure S4); 27 proteins were increased in abundance (Figure 4D and Table S6D). Both these groups of proteins show minimal overlap with the proteins that accumulated on DnaK upon TF deletion (Figure 4D). Strikingly, most of the proteins that decreased in $\Delta T/K_{His}$ cells carry predicted signal sequences (Table S6C). These proteins include numerous outer membrane β-barrel proteins, suggesting that TF has a specific role in outer membrane protein biogenesis. Indeed, $\Delta T/K_{His}$ cells proved to be sensitive to treatment with detergents like deoxycholate and the antibiotic vancomycin, which is indicative of a weakening of the outer membrane (Figure 4E) (Nichols et al., 2011). The proteins that increased in $\Delta T/K_{His}$ cells include cytosolic chaperones and proteases, as well as the ATPase SecA required for membrane translocation of outer membrane proteins (Table S6D). However, these proteins are only moderately upregulated (∼1.5-fold), suggesting that loss of TF function at 37°C causes only limited proteome stress.

These results indicate a functional redundancy of TF and DnaK in the folding/assembly of ribosomal and other small, basic proteins. In addition, TF has a specific role in the biogenesis of outer membrane β-barrel proteins. This function cannot be performed by DnaK and is only partially replaced by other chaperones, resulting in outer membrane destabilization.

Interplay of DnaK and GroEL/ES

GroEL and its cofactor GroES are upregulated in both the ΔKJ and $\Delta T/K_{His}$ cells (Tables S2 and S6D), suggesting that these chaperone systems form a functional network. Strikingly, 119 of the identified DnaK interactors are known GroEL substrates (Fujiwara et al., 2010; Kerner et al., 2005), and together these proteins amount to ∼30% of all DnaK interactors by mass. The number of GroEL substrates on DnaK increases to 152 in $\Delta T/K_{His}$ cells (Figure 5A, Table S1, and Proteome Commons Tranche repository). Forty-two of these DnaK interactors are obligate GroEL-dependent (class III) and thus must be delivered to GroEL for folding, whereas 80 belong to class II and 30 to class

I (Figure 5B). Class II substrates are highly chaperone dependent but can utilize either GroEL/ES or DnaK/DnaJ for folding in vitro, whereas class I proteins have a lower chaperone dependence (Kerner et al., 2005). About 90 of the previously identified GroEL substrates were not detected on DnaK. Many of these proteins are of low abundance and thus may have very low steady-state levels on DnaK.

To investigate how the depletion of GroEL/ES affects the spectrum of DnaK interactors, K_{His} cells carrying the *groELS* operon under arabinose control were shifted from arabinose (LS+/K_{His}) to glucose for 3.5 hr (LS−/K_{His}) at 37°C, which resulted in ∼97% depletion of GroEL/ES (Kerner et al., 2005; McLennan and Masters, 1998). Note that the cells grow normally during the first 5 hr of GroEL/ES depletion (data not shown). Ninety-two proteins increased on DnaK (2- to 60-fold) upon GroEL depletion and 54 proteins decreased (Tables S7A and S7B). The former include 38 GroEL substrates (19 class III proteins) (Figure 5B). They are enriched in domains with SCOP fold c.1 (TIM-barrel) (Figure S5A), which is prominently represented among obligate GroEL substrates (Fujiwara et al., 2010; Kerner et al., 2005) (Table S7A). The proteins depleted from DnaK include 11 GroEL substrates, mostly of class II (Table S7B), suggesting that they are partially displaced from DnaK by class III substrates that are unable to fold.

We also analyzed the consequences of GroEL depletion at the proteome level. Depletion of GroEL resulted in a ∼35%−95% decrease in abundance of 114 proteins and a $\geq$2-fold increase of 95 proteins (Tables S7C and S7D). The former include 44 GroEL substrates (24 class III proteins) (Figure 5B and Table S7C) that are apparently degraded (Figure S5B). Strikingly, 18 of these GroEL substrates nevertheless accumulated on DnaK (Figure 5C), suggesting that they are stabilized by DnaK for transfer to the degradation machinery. The proteins that are upregulated upon GroEL depletion include chaperones and proteases (upregulated ∼2-fold) as well as 19 GroEL substrates (Table S7C). In addition to degradation, loss of GroEL function at 37°C also resulted in substantial aggregation of many obligate GroEL substrates (Figure 5D) (Chapman et al., 2006; Kerner et al., 2005).

In summary, GroEL substrates interact extensively with DnaK. Upon depletion of GroEL, obligate GroEL substrates accumulate further on DnaK and are either transferred to the degradation machinery or eventually aggregate.

Proteostasis Collapse upon Combined Deletion of DnaK and TF

Prevention of protein aggregation is considered fundamental to proteostasis maintenance (Hartl et al., 2011). To define the relative contribution of the different chaperone systems to aggregation prevention, we performed a comparative analysis of the aggregated proteomes upon individual and combined chaperone deletion at 30°C, where cells lacking DnaK/DnaJ and TF (ΔKJT) still grow, albeit slowly (Figure 1B and Figure S1A). As described above, 474 proteins increased significantly in the insoluble fraction of ΔKJ cells, compared to only 15 proteins in $\Delta T/K_{His}$ cells and 33 proteins in GroEL/ES depleted (LS−/K_{His}) cells (Figure 6A and Table S8), indicating a major role of the DnaK system in aggregation prevention. Upon combined deletion of DnaK/DnaJ and TF, 1,087 proteins aggregated, including 403 DnaK interactors identified in this study (Figure 6A and
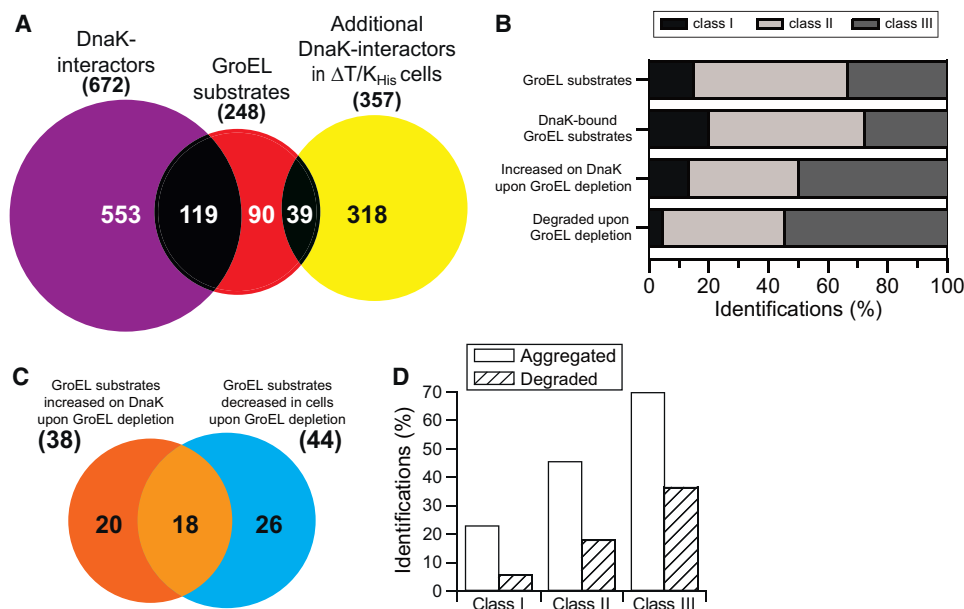
Figure 5. GroEL Substrates Accumulate on DnaK in GroEL-Depleted Cells

(A) Overlap of previously identified GroEL substrates (248 proteins) (Kerner et al., 2005) with DnaK interactors in K_{His} (672 proteins) and $\Delta T/K_{His}$ (357 additional DnaK interactors).

(B) Class distribution of the GroEL substrates (Kerner et al., 2005) compared to the class distribution of GroEL substrates bound to DnaK in K_{His} cells, increased on DnaK upon GroEL-depletion and class distribution of GroEL substrates that are partially degraded in total cell lysate upon GroEL-depletion. Class I, chaperone independent; class II, chaperone dependent; class III, obligate GroEL substrates.

(C) Overlap of the GroEL substrates that are significantly decreased in the proteome of LS−/K_{His} cells due to degradation and that increase on DnaK upon GroEL-depletion.

(D) Class distribution of GroEL substrates identified at 37°C in the aggregate fraction of LS−/K_{His} cells and of GroEL substrates decreased in the total proteome of LS−/K_{His} cells due to degradation.

Table S8). The aggregated proteins also included 149 of a total of 196 proteins shown previously to aggregate in cells lacking DnaK/DnaJ and TF (Deuerling et al., 2003; Martinez-Hackert and Hendrickson, 2009). Moreover, whereas in ΔKJ cells only 65 proteins aggregated substantially (>5% depletion from the soluble fraction), the number of substantially aggregated proteins increased 4-fold upon additional loss of TF (Figure 6A and Table S8). Strikingly, the size distribution of these proteins showed a strong shift to large proteins >50 KDa, frequently containing multiple domains (Figure 6B and Table S8). Many of these proteins (~50%) are identified DnaK substrates of average or above average abundance (Table S1) and represent a subset of the large proteins that interact with DnaK on synthesis (Figure 3B). Apparently, these proteins are chaperone-dependent but can utilize either the DnaK system or TF for efficient folding.

Remarkably, ~70% of the previously identified GroEL substrates (167 proteins) (Kerner et al., 2005) were also recovered in the aggregate fraction of ΔKJT cells (Figure 6A), many of which aggregated substantially (Table S8). This effect was observed despite a ~10-fold upregulation of GroEL/ES (data not shown). Aggregation of GroEL substrates was essentially undetectable in ΔKJ or ΔT/K_{His} cells at 30°C (Table S8). Thus, substrate delivery to GroEL critically depends on the upstream chaperones but can be performed by either DnaK or TF.

A large number of ribosomal proteins also accumulated in the insoluble fraction of ΔKJT cells, almost all of which were identi-

fied as DnaK interactors (Table S8). Deletion of DnaK/DnaJ alone resulted in the aggregation of only three ribosomal proteins, whereas none of these aggregated in the ΔT/K_{His} cells. Although aggregation did not cause a significant depletion of ribosomal proteins from the soluble fraction, these results suggested that ΔKJT cells have a defect in ribosomal biogenesis. Indeed, numerous ribosomal proteins were reduced in abundance by 10%−30% in total lysates of ΔKJT cells compared to K_{His} cells and the single chaperone deletions (Figure 6C). Interestingly, two small ribosomal proteins (RpsQ S17 and RpsT S20) were increased in abundance, an effect that was also detected in ΔKJ cells (Figure 6C).

In summary, the combined loss of DnaK/DnaJ and TF results in a pronounced proteostasis collapse characterized by the aggregation of large, multidomain proteins, disruption of proper protein flux through GroEL/ES and defective ribosomal biogenesis. These findings explain the strong growth defect of ΔKJT cells at 30°C and their inability to grow at higher temperatures.

DISCUSSION

The DnaK Interactome
The DnaK interactome characterized here comprises at least ~700 proteins in WT cells and ~1,000 proteins in TF-deleted cells, demonstrating the pervasive role of the Hsp70 chaperone system in protein folding and proteostasis. While the vast
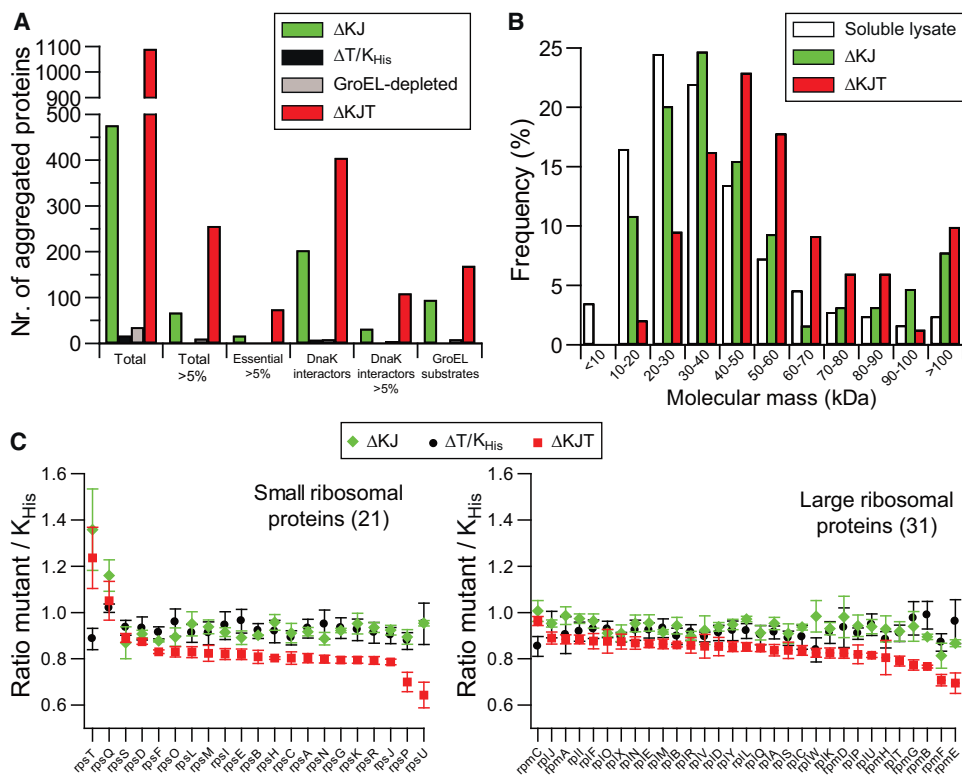
Figure 6. Proteostasis Collapse in Δ*dnaKdnaJ*/Δ*tig* Cells

(A) Protein aggregation in ΔKJ, ΔT/K$_{His}$, LS−/K$_{His}$, and ΔKJT cells. The number of aggregated proteins were analyzed according to the following categories: total, aggregated to >5% (Total > 5%), essential proteins aggregated to >5% (Essential > 5%), DnaK interactors, DnaK interactors aggregated to >5% and GroEL substrates.

(B) Size distribution of >5% aggregated proteins in ΔKJ and ΔKJT cells in comparison to soluble lysate proteins of WT cells.

(C) Changes in abundance of small and large ribosomal proteins in ΔKJ, ΔT/K$_{His}$, and ΔKJT relative to K$_{His}$ cells. SILAC ratios (mutant/K$_{His}$) are shown with standard deviations from three independent experiments for 21 small and 31 large ribosomal proteins.

majority of DnaK substrates (∼80%) are cytosolic, DnaK also interacts with a small subset of proteins of the inner membrane, periplasm and outer membrane. Under conditions of exponential cell growth at 37°C, proteins bind to DnaK preferentially upon synthesis and may return to DnaK during their life time for conformational maintenance.

The dependence of proteins on DnaK for folding or maintenance is partially buffered by TF and other chaperones, but is reflected by the relative enrichment of substrates on DnaK. By measuring for each protein the fraction of total that is chaperone-bound, we defined a set of ∼180 interactors that are highly enriched on DnaK and amount to about 40% of the total mass of DnaK substrates. DnaK-enriched proteins are generally of average or below average cellular abundance and of low solubility. Essential proteins are underrepresented among this group. DnaK dependence tends to correlate with the number of predicted DnaK binding sites in polypeptide sequences, and the propensity of proteins to populate structurally dynamic intermediates. Moreover, proteins that interact extensively with DnaK are often part of heterooligomeric complexes (Figure 7A).

Our findings suggest that proteins of lower abundance are frequently prone to misfolding or aggregation and thus have high chaperone requirements (with dependence on a specific

chaperone system), whereas the folding properties of abundant (and often essential) proteins have been optimized in evolution, resulting in a reduced (or less specific) chaperone requirement. This is consistent with the existence of a negative correlation between the calculated aggregation-propensity of proteins and their cellular abundance (Tartaglia et al., 2010; Tartaglia et al., 2007). Indeed, the less abundant, DnaK-enriched substrates are aggregation-prone upon translation in vitro (Niwa et al., 2009) and are either degraded or aggregate in the absence of DnaK in vivo, reflecting their specific requirement for DnaK for folding and conformational maintenance. Interestingly, several DnaK-enriched substrates contain at least one domain with SCOP fold c.37 (Figure 7A). Proteins with this and other complex α/β topologies have to form many long-range interactions during folding and are thus likely to populate dynamic folding intermediates exposing hydrophobic residues (Gromiha and Selvaraj, 2004). Moreover, proteins with c.37 domains often assemble into heterooligomeric complexes (Figure S2G), a process that may be facilitated by DnaK's ability to bind partially structured protein regions in addition to extended peptide segments (Schlecht et al., 2011). On the other hand, many large proteins of higher cellular abundance but lower enrichment on DnaK are adapted to utilize either DnaK or TF for de novo folding. These
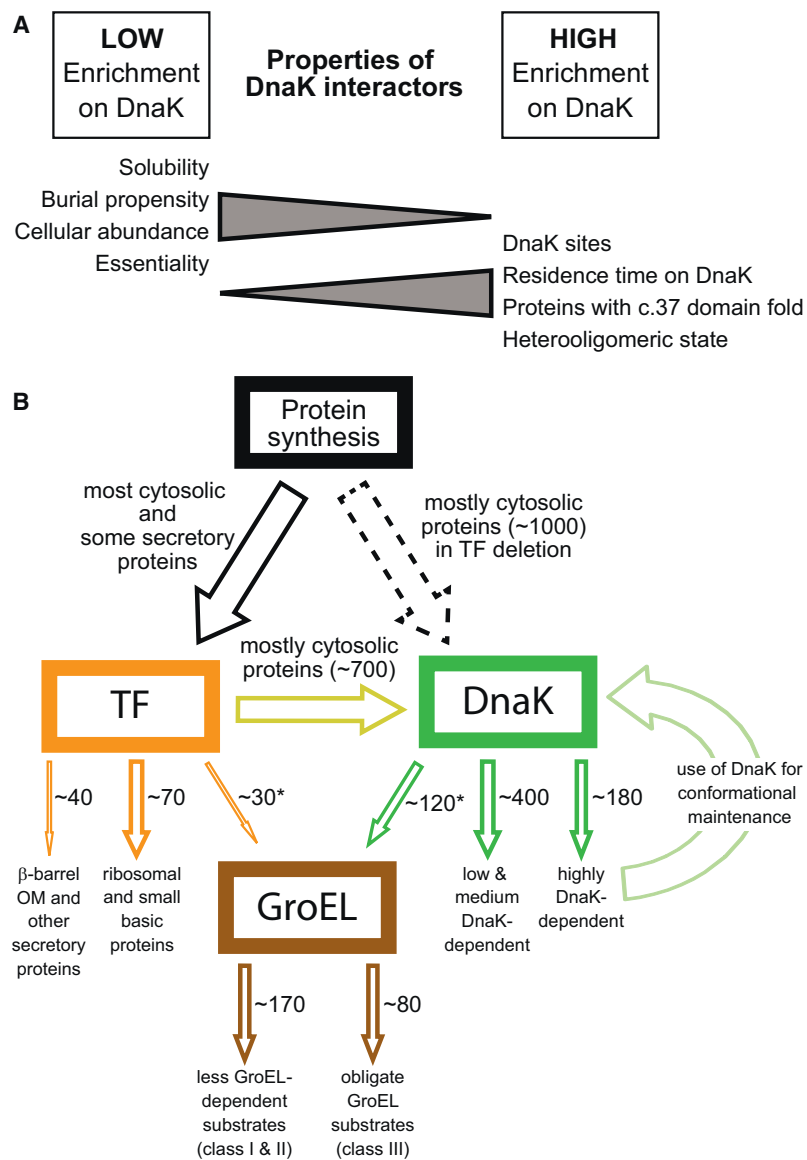
Figure 7. Central Role of DnaK in the Cytosolic Chaperone Network

(A) Properties of DnaK substrates correlating with their relative enrichment on DnaK (fraction of total cellular protein bound to DnaK).

(B) Functional redundancies and specificities in the chaperone network formed by TF, the DnaK system, and GroEL. Numbers denote numbers of proteins determined in this work and in the study by Kerner et al. (2005). *Note that ~100 known GroEL substrates were either not or not reproducibly identified as DnaK interactors. These proteins are of low cellular abundance and thus may have very low steady-state levels on DnaK.

30% of total in the absence of DnaK/DnaJ already at 30°C. The sensitivity of Δ*dnaK* cells to antibiotics inhibiting protein synthesis (Nichols et al., 2011) would correlate with the extensive interaction of DnaK with ribosomal proteins and the degradation in ΔKJ cells of several DnaK interactors of COG class E (amino acid transport and metabolism). Finally, the sensitivity of Δ*dnaK* cells to acidic conditions (Nichols et al., 2011) is consistent with the 80%−97% degradation in ΔKJ cells of the periplasmic chaperones of acid-denatured proteins, hdeA, and hdeB.

Interplay between Chaperone Modules

Our analysis of the DnaK interactome in cells lacking TF or depleted of GroEL/ES underscores the significance of DnaK as a central hub in the chaperone network. The observed accumulation of a subset of proteins on DnaK in the absence of TF defines in a quantitative manner the functional redundancy between these two chaperone systems described earlier (Deuerling et al., 1999; Teter et al., 1999). Interestingly, these substrates comprise mostly ribosomal and other small (<20 kDa), positively charged proteins (Figure 7B), which may normally interact predominantly with TF, but shift to DnaK when TF is absent. Indeed, TF has a negative net charge (Ferbitz et al., 2004; Martinez-Hackert and Hendrickson, 2009), which may facilitate its interaction with positively charged nascent polypeptides, and a role of TF in the folding/assembly of ribosomal proteins has been suggested (Martinez-Hackert and Hendrickson, 2009).

In contrast, the DnaK system is unable to replace the role of TF in the biogenesis of a set of secretory proteins, prominently including β-barrel proteins of the outer membrane (Figure 7B). These proteins undergo partial degradation in cells lacking TF, suggesting a specific role of TF in translocation of outer membrane preproteins across the inner membrane. Such a function of TF would be consistent with the initial identification of TF as a chaperone of proOmpA translocation in vitro (Crooke et al., 1988) and with the finding that TF modulates the kinetics of

proteins aggregate substantially only in the absence of both chaperones, defining sequence length, and hence multidomain topology, as a property strongly correlated with chaperone dependence.

Proteins with essential functions are underrepresented among the DnaK-enriched substrates. However, our identification of the essential tubulin homolog, FtsZ, and the cooperating MinCDE proteins as strong DnaK binders (Table S1) would explain why DnaK mutant cells have defects in cell division (Bukau and Walker, 1989). Furthermore, the sensitivity of Δ*dnaK* cells to antibiotics causing DNA damage (Nichols et al., 2011) is consistent with the finding that proteins of COG class L (DNA replication, recombination and repair), such as the nucleotide excision repair protein UvrA, are overrepresented among the DnaK-enriched substrates (Figure S2). UvrA is a large, heterooligomeric protein with two c.37 domains; which aggregates to

protein export (Lee and Bernstein, 2002; Ullers et al., 2007). It is also of interest in this context that TF structurally resembles the periplasmic chaperone for outer membrane proteins, SurA (Bitto and McKay, 2002; Ferbitz et al., 2004).

An effective functional cooperation apparently exists between TF and the DnaK system in the folding of a group of large multi-domain proteins that aggregate substantially only in the absence of both chaperones. These proteins may normally interact sequentially with TF and DnaK during translation or with multiple TF molecules in the absence of DnaK, as shown with large model proteins in vitro (Agashe et al., 2004; Kaiser et al., 2006). Notably, most of these proteins would be unable to interact productively with GroEL, as the capacity of the GroEL/ES folding compartment is limited to proteins up to ∼60 kDa (Kerner et al., 2005).

The DnaK interactome overlaps extensively with the set of previously identified GroEL substrates (Figure 7B), most of which are below 50 kDa in size (Kerner et al., 2005). GroEL substrates amount to nearly 30% of the total mass of DnaK interactors, indicating that protein transfer between DnaK and GroEL is a central function of the chaperone network. We estimate that only a minor fraction of GroEL substrates (∼20%) are transferred directly from TF to GroEL, circumventing DnaK (Figure 7B). Notably, upon GroEL-depletion, obligate GroEL substrates accumulate further on DnaK, reflecting an important role of DnaK as a buffer in stabilizing these proteins until GroEL is available or in transferring them to the proteolytic system.

Defining Proteostasis Collapse

Upon growth at 30°C, the loss of individual chaperone modules—DnaK/DnaJ, TF or GroEL/ES—is remarkably well tolerated by *E. coli* cells in terms of preventing major protein aggregation. Instead, degradation is the strongly preferred fate of misfolded proteins under these conditions (Tables S2B, S6C, and S7C). However, proteostasis collapse characterized by extensive aggregation of relatively abundant proteins occurs when TF is deleted in addition to DnaK/DnaJ. Apparently, the chaperone capacity available for the folding and stabilization of large proteins in particular becomes severely limiting and, as a result, aggregation is favored relative to degradation. Furthermore, our data show that the loss of the upstream chaperones, TF and DnaK/DnaJ, disrupts the normal protein flux to GroEL, resulting in wide-spread aggregation of GroEL-substrates, despite a ∼10-fold upregulation of GroEL under these conditions. The failure of newly synthesized GroEL substrates to reach the abundantly expressed chaperonin signifies the systematic collapse of the chaperone network.

EXPERIMENTAL PROCEDURES

Bacterial Strains
The *E. coli* strains used were based on MC4100 (WT) and are described in Extended Experimental Procedures.

Isolation of DnaK-Interactor Complexes
SILAC labeling of cells was performed at 37°C in M63 medium supplemented with light (L), medium (M), or heavy (H) arginine and lysine isotopes (see Extended Experimental Procedures). DnaK interactors were isolated from cells growing exponentially (OD$_{600nm}$ ∼1). In pulse-SILAC experiments, L-labeled cells were shifted to M-medium for 2.5 min; in pulse chase-SILAC experi-

ments, L-labeled cells were shifted to H-medium for 2 min and then chased by addition of a 100-fold excess of L arginine and lysine for 2, 4, and 8 min. Spheroplasts were prepared as described (Ewalt et al., 1997) and lysed in hypo-osmotic buffer containing apyrase. Soluble cell lysate was prepared by centrifugation (20,000 × g, 30 min). Talon beads (Invitrogen) were used to isolate the DnaK-His6 and its interactors. The eluates containing bound proteins obtained from equal amounts of L-, M-, or H-labeled cells were mixed (see Extended Experimental Procedures). Samples were prepared for LC-MS/MS as described (Figure 1C) (Ong and Mann, 2006). The spectra were interpreted using MaxQuant version 1.0.13.13 (Cox and Mann, 2008) combined with Mascot version 2.2 (Matrix Science, www.matrixscience.com).

The MaxQuant tables along with a full list of identified proteins and quantitations are available at the Proteome Commons Tranche repository (https://proteomecommons.org/) by inserting the following tranche code: RKuFJcuu8iBnZHlBN4Nth0pz+HQgPNvV0zJvdnMN8wyAN8l7ifufEnmW6j2C wn0msEakFC6eulEqlYv+7B+dFALonrgAAAAAAAAKDA== and passphrase: vqXGUF93rGLCraqm1yll.

The raw data is accessible using tranche codes and passphrase given in Extended Experimental Procedures.

Fractionation of Total Cell Lysate
E. coli MC4100 *dnaK-His6* (K$_{His}$) and chaperone mutant strains were grown to OD$_{600nm}$ ∼1 at 30°C or 37°C, as indicated, in the respective SILAC medium. Cells were collected, flash frozen, and lysed by sonication. Whole proteome analyses on total lysates, soluble, and detergent insoluble fractions (Deuerling et al., 2003) were performed by LC-MS/MS as described in Extended Experimental Procedures.

Bioinformatic Analysis
Bioinformatics and statistical analyses of the physico-chemical properties of protein sequences were performed as detailed in Extended Experimental Procedures. Note that both DnaJ and GrpE, the cofactors of DnaK, are excluded in all bioinformatic analyses.

SUPPLEMENTAL INFORMATION

Supplemental Information includes Extended Experimental Procedures, five figures, and eight tables and can be found with this article online at doi:10.1016/j.celrep.2011.12.007.

LICENSING INFORMATION

ACKNOWLEDGMENTS

REFERENCES

Agashe, V.R., Guha, S., Chang, H.C., Genevaux, P., Hayer-Hartl, M., Stemp, M., Georgopoulos, C., Hartl, F.U., and Barral, J.M. (2004). Function of trigger factor and DnaK in multidomain protein folding: increase in yield at the expense of folding speed. Cell *117*, 199–209.

Balch, W.E., Morimoto, R.I., Dillin, A., and Kelly, J.W. (2008). Adapting proteostasis for disease intervention. Science *319*, 916–919.

Bitto, E., and McKay, D.B. (2002). Crystallographic structure of SurA, a molecular chaperone that facilitates folding of outer membrane porins. Structure *10*, 1489–1498.

Bukau, B., and Walker, G.C. (1989). Cellular defects caused by deletion of the *Escherichia coli* dnaK gene indicate roles for heat shock protein in normal metabolism. J. Bacteriol. *171*, 2337–2346.

Chapman, E., Farr, G.W., Usaite, R., Furtak, K., Fenton, W.A., Chaudhuri, T.K., Hondorp, E.R., Matthews, R.G., Wolf, S.G., Yates, J.R., et al. (2006). Global aggregation of newly translated proteins in an Escherichia coli strain deficient of the chaperonin GroEL. Proc. Natl. Acad. Sci. USA *103*, 15800–15805.

Cox, J., and Mann, M. (2008). MaxQuant enables high peptide identification rates, individualized p.p.b.-range mass accuracies and proteome-wide protein quantification. Nat. Biotechnol. *26*, 1367–1372.

Crooke, E., Guthrie, B., Lecker, S., Lill, R., and Wickner, W. (1988). ProOmpA is stabilized for membrane translocation by either purified E. coli trigger factor or canine signal recognition particle. Cell *54*, 1003–1011.

Deuerling, E., Patzelt, H., Vorderwülbecke, S., Rauch, T., Kramer, G., Schaffitzel, E., Mogk, A., Schulze-Specking, A., Langen, H., and Bukau, B. (2003). Trigger Factor and DnaK possess overlapping substrate pools and binding specificities. Mol. Microbiol. *47*, 1317–1328.

Deuerling, E., Schulze-Specking, A., Tomoyasu, T., Mogk, A., and Bukau, B. (1999). Trigger factor and DnaK cooperate in folding of newly synthesized proteins. Nature *400*, 693–696.

Ewalt, K.L., Hendrick, J.P., Houry, W.A., and Hartl, F.U. (1997). In vivo observation of polypeptide flux through the bacterial chaperonin system. Cell *90*, 491–500.

Ferbitz, L., Maier, T., Patzelt, H., Bukau, B., Deuerling, E., and Ban, N. (2004). Trigger factor in complex with the ribosome forms a molecular cradle for nascent proteins. Nature *431*, 590–596.

Fujiwara, K., Ishihama, Y., Nakahigashi, K., Soga, T., and Taguchi, H. (2010). A systematic survey of in vivo obligate chaperonin-dependent substrates. EMBO J. *29*, 1552–1564.

Gamer, J., Bujard, H., and Bukau, B. (1992). Physical interaction between heat shock proteins DnaK, DnaJ, and GrpE and the bacterial heat shock transcription factor sigma 32. Cell *69*, 833–842.

Genevaux, P., Keppel, F., Schwager, F., Langendijk-Genevaux, P.S., Hartl, F.U., and Georgopoulos, C. (2004). In vivo analysis of the overlapping functions of DnaK and trigger factor. EMBO Rep. *5*, 195–200.

Gerdes, S.Y., Scholle, M.D., Campbell, J.W., Balázsi, G., Ravasz, E., Daugherty, M.D., Somera, A.L., Kyrpides, N.C., Anderson, I., Gelfand, M.S., et al. (2003). Experimental determination and system level analysis of essential genes in Escherichia coli MG1655. J. Bacteriol. *185*, 5673–5684.

Gidalevitz, T., Prahlad, V., and Morimoto, R.I. (2011). The stress of protein misfolding: from single cells to multicellular organisms. Cold Spring Harb. Perspect. Biol. *3*, 3.

Gromiha, M.M., and Selvaraj, S. (2004). Inter-residue interactions in protein folding and stability. Prog. Biophys. Mol. Biol. *86*, 235–277.

Hartl, F.U., Bracher, A., and Hayer-Hartl, M. (2011). Molecular chaperones in protein folding and proteostasis. Nature *475*, 324–332.

Hartl, F.U., and Hayer-Hartl, M. (2009). Converging concepts of protein folding in vitro and in vivo. Nat. Struct. Mol. Biol. *16*, 574–581.

Ishihama, Y., Oda, Y., Tabata, T., Sato, T., Nagasu, T., Rappsilber, J., and Mann, M. (2005). Exponentially modified protein abundance index (emPAI) for estimation of absolute protein amount in proteomics by the number of sequenced peptides per protein. Mol. Cell. Proteomics *4*, 1265–1272.

Janin, J. (1979). Surface and inside volumes in globular proteins. Nature *277*, 491–492.

Kaiser, C.M., Chang, H.C., Agashe, V.R., Lakshmipathy, S.K., Etchells, S.A., Hayer-Hartl, M., Hartl, F.U., and Barral, J.M. (2006). Real-time observation of trigger factor function on translating ribosomes. Nature *444*, 455–460.

Kerner, M.J., Naylor, D.J., Ishihama, Y., Maier, T., Chang, H.C., Stines, A.P., Georgopoulos, C., Frishman, D., Hayer-Hartl, M., Mann, M., and Hartl, F.U. (2005). Proteome-wide analysis of chaperonin-dependent protein folding in Escherichia coli. Cell *122*, 209–220.

Lee, H.C., and Bernstein, H.D. (2002). Trigger factor retards protein export in Escherichia coli. J. Biol. Chem. *277*, 43527–43535.

Maki, J.A., Schnobrich, D.J., and Culver, G.M. (2002). The DnaK chaperone system facilitates 30S ribosomal subunit assembly. Mol. Cell *10*, 129–138.

Martinez-Hackert, E., and Hendrickson, W.A. (2009). Promiscuous substrate recognition in folding and assembly activities of the trigger factor chaperone. Cell *138*, 923–934.

Mayer, M.P. (2010). Gymnastics of molecular chaperones. Mol. Cell *39*, 321–331.

McLennan, N., and Masters, M. (1998). GroE is vital for cell-wall synthesis. Nature *392*, 139.

Nichols, R.J., Sen, S., Choo, Y.J., Beltrao, P., Zietek, M., Chaba, R., Lee, S., Kazmierczak, K.M., Lee, K.J., Wong, A., et al. (2011). Phenotypic landscape of a bacterial cell. Cell *144*, 143–156.

Niwa, T., Ying, B.W., Saito, K., Jin, W., Takada, S., Ueda, T., and Taguchi, H. (2009). Bimodal protein solubility distribution revealed by an aggregation analysis of the entire ensemble of Escherichia coli proteins. Proc. Natl. Acad. Sci. USA *106*, 4201–4206.

Ong, S.E., Blagoev, B., Kratchmarova, I., Kristensen, D.B., Steen, H., Pandey, A., and Mann, M. (2002). Stable isotope labeling by amino acids in cell culture, SILAC, as a simple and accurate approach to expression proteomics. Mol. Cell. Proteomics *1*, 376–386.

Ong, S.E., and Mann, M. (2006). A practical recipe for stable isotope labeling by amino acids in cell culture (SILAC). Nat. Protoc. *1*, 2650–2660.

Raineri, E., Ribeca, P., Serrano, L., and Maier, T. (2010). A more precise characterization of chaperonin substrates. Bioinformatics *26*, 1685–1689.

René, O., and Alix, J.-H. (2011). Late steps of ribosome assembly in E. coli are sensitive to a severe heat stress but are assisted by the HSP70 chaperone machine. Nucleic Acids Res. *39*, 1855–1867.

Rüdiger, S., Buchberger, A., and Bukau, B. (1997). Interaction of Hsp70 chaperones with substrates. Nat. Struct. Biol. *4*, 342–349.

Schlecht, R., Erbse, A.H., Bukau, B., and Mayer, M.P. (2011). Mechanics of Hsp70 chaperones enables differential interaction with client proteins. Nat. Struct. Mol. Biol. *18*, 345–351.

Smock, R.G., Rivoire, O., Russ, W.P., Swain, J.F., Leibler, S., Ranganathan, R., and Gierasch, L.M. (2010). An interdomain sector mediating allostery in Hsp70 molecular chaperones. Mol. Syst. Biol. *6*, 414.

Straus, D., Walter, W., and Gross, C.A. (1990). DnaK, DnaJ, and GrpE heat shock proteins negatively regulate heat shock gene expression by controlling the synthesis and stability of sigma 32. Genes Dev. *4*(12A), 2202–2209.

Tartaglia, G.G., Dobson, C.M., Hartl, F.U., and Vendruscolo, M. (2010). Physicochemical determinants of chaperone requirements. J. Mol. Biol. *400*, 579–588.

Tartaglia, G.G., Pawar, A.P., Campioni, S., Dobson, C.M., Chiti, F., and Vendruscolo, M. (2008). Prediction of aggregation-prone regions in structured proteins. J. Mol. Biol. *380*, 425–436.

Tartaglia, G.G., Pechmann, S., Dobson, C.M., and Vendruscolo, M. (2007). Life on the edge: a link between gene expression levels and aggregation rates of human proteins. Trends Biochem. Sci. *32*, 204–206.

Teter, S.A., Houry, W.A., Ang, D., Tradler, T., Rockabrand, D., Fischer, G., Blum, P., Georgopoulos, C., and Hartl, F.U. (1999). Polypeptide flux through bacterial Hsp70: DnaK cooperates with trigger factor in chaperoning nascent chains. Cell *97*, 755–765.

Ullers, R.S., Ang, D., Schwager, F., Georgopoulos, C., and Genevaux, P. (2007). Trigger Factor can antagonize both SecB and DnaK/DnaJ chaperone functions in Escherichia coli. Proc. Natl. Acad. Sci. USA *104*, 3101–3106.

Van Durme, J., Maurer-Stroh, S., Gallardo, R., Wilkinson, H., Rousseau, F., and Schymkowitz, J. (2009). Accurate prediction of DnaK-peptide binding via homology modelling and experimental data. PLoS Comput. Biol. *5*, e1000475.

Yu, N.Y., Laird, M.R., Spencer, C., and Brinkman, F.S. (2011). PSORTdb—an expanded, auto-updated, user-friendly protein subcellular localization database for Bacteria and Archaea. Nucleic Acids Res. *39*(Database issue), D241–D244.

Zhao, K., Liu, M., and Burgess, R.R. (2005). The global transcriptional response of Escherichia coli to induced σ^{32} protein involves σ^{32} regulon activation followed by inactivation and degradation of σ^{32} in vivo. J. Biol. Chem. *280*, 17758–17768.

Zhu, X.T., Zhao, X., Burkholder, W.F., Gragerov, A., Ogata, C.M., Gottesman, M.E., and Hendrickson, W.A. (1996). Structural analysis of substrate binding by the molecular chaperone DnaK. Science *272*, 1606–1614.

Zhuravleva, A., and Gierasch, L.M. (2011). Allosteric signal transmission in the nucleotide-binding domain of 70-kDa heat shock protein (Hsp70) molecular chaperones. Proc. Natl. Acad. Sci. USA *108*, 6987–6992.